

Qualitative Stability and Synchronicity Analysis of Power Network Models in Port-Hamiltonian form

Volker Mehrmann* and Riccardo Morandin† and Simona Olmi‡ and
Eckehard Schöll§

October 5, 2018

Abstract

In view of highly decentralized and diversified power generation concepts, in particular with renewable energies such as wind and solar power, the analysis and control of the stability and the synchronization of power networks is an important topic that requires different levels of modeling detail for different tasks. A frequently used qualitative approach relies on simplified nonlinear network models like the Kuramoto model. Although based on basic physical principles, the usual formulation in form of a system of coupled ordinary differential equations is not always adequate. We present a new energy-based formulation of the Kuramoto model as port-Hamiltonian system of differential-algebraic equations. This leads to a very robust representation of the system with respect to disturbances, it encodes the underlying physics, such as the dissipation inequality or the deviation from synchronicity, directly in the structure of the equations, it explicitly displays all possible constraints and allows for robust simulation methods. Due to its systematic energy based formulation the model class allows easy extension, when further effects have to be considered, higher fidelity is needed for qualitative analysis, or the system needs to be coupled in a robust way to other networks. We demonstrate the advantages of the modified modeling approach with analytic results and numerical experiments.

1 Introduction

The increased percentage of renewable energies, such as wind and solar power, and the decentralization of power generation makes the stability and synchronization control of modern power systems increasingly difficult. To address different control and optimization tasks, there are many different approaches to model power networks; we will briefly present a power grid model hierarchy of differential-algebraic systems. At the lowest levels of such a model hierarchy simplified nonlinear network models like the Kuramoto model are placed which are often used for a qualitative analysis of the network behavior [10, 16].

The usual formulation of the Kuramoto model in form of a coupled system of ordinary differential equations as in [8, 10, 16, 22, 23, 24, 21, 9] is, however, not always appropriate, because physical properties like the conservation of energy and momentum, or Kirchoff's node conditions are only

*Institut für Mathematik MA 4-5, TU Berlin, Str. des 17. Juni 136, D-10623 Berlin, FRG. *Email address:* mehrmann@math.tu-berlin.de. Supported by Deutsche Forschungsgemeinschaft via Project A2 within SFB 910 and by *Einstein Foundation Berlin* via the Einstein Center ECMath.

†Institut für Mathematik MA 4-5, TU Berlin, Str. des 17. Juni 136, D-10623 Berlin, FRG. *Email address:* morandin@math.tu-berlin.de. Supported by *Einstein Foundation Berlin* via the Einstein Center ECMath.

‡Institut für Theoretische Physik, Sekr. EW 7-1, TU Berlin, Hardenbergstr. 36, D-10623 Berlin, FRG & CNR - Consiglio Nazionale delle Ricerche - Istituto dei Sistemi Complessi, 50019, Sesto Fiorentino, Italy. *Email address:* simona.olmi@gmail.com. Supported by Deutsche Forschungsgemeinschaft via Project A1 within SFB 910.

§Institut für Theoretische Physik, Sekr. EW 7-1, TU Berlin, Hardenbergstr. 36, D-10623 Berlin, FRG. *Email address:* schoell@physik.tu-berlin.de. Supported by Deutsche Forschungsgemeinschaft via Project A1 within SFB 910.

implicitly represented in the equations, and thus in numerical simulation or control methods they may be violated and lead to un-physical behavior. To prevent this, we present a new energy-based formulation of the Kuramoto model as port-Hamiltonian system of differential-algebraic equations. This model is a very robust representation of the system with respect to disturbances, since it encodes the underlying laws of physics in the algebraic and geometric structure of the equations. It allows the development of structure preserving methods that satisfy the physical laws after discretization and in finite precision arithmetic leading to robust simulation and control methods. The energy-based modeling approach allows for easy model refinement, as well as interconnection with other systems from different physical domains. We illustrate the new modeling approach with analytic results and numerical experiments and indicate how this approach can be generalized to also allow quantitative analysis.

The basis for our approach are *differential-algebraic equations (DAEs)*, also called *descriptor systems* in the control context. They have become a paradigm for the modeling of systems in different physical domains and they are incorporated in automated modeling frameworks such as MODELICA*. Descriptor systems allow the explicit representation of constraints and interfaces in the model. In the most general nonlinear setting they have the form

$$F(t, x, \dot{x}, u) = 0, \quad (1)$$

typically together with an initial condition $x(t_0) = x_0$ and an output equation

$$y = G(t, x, u). \quad (2)$$

Here, denoting by $C^0(\mathbb{I}, \mathbb{R}^m)$ the set of continuous functions from a compact time interval $\mathbb{I} \subseteq \mathbb{R}$ to \mathbb{R}^m , the function x represents the state, u the input, and y the output of the system. Although more general function spaces can be considered, we assume that $F \in C^0(\mathbb{I} \times \mathbb{D}_x \times \mathbb{D}_{\dot{x}} \times \mathbb{D}_u, \mathbb{R}^\ell)$ is sufficiently smooth, and that $\mathbb{D}_x, \mathbb{D}_{\dot{x}} \subseteq \mathbb{R}^n$, $\mathbb{D}_u \subseteq \mathbb{R}^m$, $\mathbb{D}_y \subseteq \mathbb{R}^p$ are open sets. This most general form of descriptor system is used in the general mathematical analysis and general numerical methods, see [17], but it does not display the explicit constraints, e. g. balance laws, or interface conditions. Furthermore, there may exist hidden constraints or consistency requirements, which makes further reformulations or regularizations necessary, see [5, 17, 20].

Another important recent development is the use of *energy based modeling* via bond graphs [3, 7], as implemented in the automated modeling package 20-SIM†. The resulting systems have a *port-Hamiltonian (pH) structure*, see e.g. [11, 15, 25, 27, 28], that encodes the underlying physical principles, such as conservation laws, passivity, or stability directly into the algebraic and geometric structure of the system model. Ordinary *pH systems* have the form

$$\begin{aligned} \dot{x} &= (J - R) \nabla_x \mathcal{H}(x) + (B - P)u, \\ y &= (B + P)^T \nabla_x \mathcal{H}(x) + (S + N)u. \end{aligned} \quad (3)$$

Here the *Hamiltonian function* $\mathcal{H}(x)$ describes the distribution of internal energy among energy storage elements of the system; $J = -J^T \in \mathbb{R}^{n,n}$ is the *structure matrix* describing energy flux among energy storage elements within the system; $R = R^T \in \mathbb{R}^{n,n}$ is the *dissipation matrix* describing energy dissipation/loss in the system; $B \pm P \in \mathbb{R}^{n,m}$ are *port matrices*, describing the manner in which energy enters and exits the system, and $S + N$, with $S = S^T \in \mathbb{R}^{m,m}$ and $N = -N^T \in \mathbb{R}^{m,m}$, describes the direct *feed-through* from input to output. All coefficients J, R, B, S, N can depend on the state x and also explicitly on the time t and also can be infinite dimensional operators. Furthermore, for pH systems it is required that

$$W = \begin{bmatrix} R & P \\ P^T & S \end{bmatrix} \geq 0, \quad (4)$$

*<https://www.modelica.org/>

†<http://www.20sim.com/>

where we write $W > 0$ (or $W \geq 0$) to denote that a real symmetric matrix W is positive definite (or positive semi-definite). In contrast to *Hamiltonian systems*, the *conservation of energy* for Hamiltonian systems is replaced by the *dissipation inequality*

$$\mathcal{H}(x(t_1)) - \mathcal{H}(x(t_0)) \leq \int_{t_0}^{t_1} y(t)^T u(t) dt, \quad (5)$$

which shows that (3) is a *passive* system, see [4] and, since $\mathcal{H}(x)$ defines a Lyapunov function, (minimal in the sense of system theory) pH systems are implicitly Lyapunov stable [14, 31, 32]. A major advantage of pH systems in the context of power system modeling is that pH systems are closed under *power-conserving interconnection*, which allows to build-up models in a modularized way, see [6], and Galerkin projection [1, 13, 26], which allows systematic discretization and model reduction.

To include interface conditions or node conditions like Kirchhoff's laws in a pH system, in [2, 29] ordinary pH systems have been extended to *port-Hamiltonian differential-algebraic equations* (*descriptor systems*) (pHDAEs), leading to the following definition, which we present here in the general linear time-varying form.

Definition 1. *A linear variable coefficient descriptor system of the form*

$$\begin{aligned} E\dot{x} &= [(J - R)Q - ET]x + (B - P)u, \\ y &= (B + P)^T Qx + (S + N)u, \end{aligned} \quad (6)$$

with $E, Q \in C^1(\mathbb{I}, \mathbb{R}^{n,n})$, $J, R, T \in C^0(\mathbb{I}, \mathbb{R}^{n,n})$, $B, P \in C^0(\mathbb{I}, \mathbb{R}^{n,m})$, $S = S^T, N = -N^T \in C^0(\mathbb{I}, \mathbb{R}^{m,m})$ is called port-Hamiltonian differential-algebraic system (pHDAE) if the following properties are satisfied:

i) For all $t \in \mathbb{I}$, $Q^T(t)E(t) = E^T(t)Q(t) \in C^1(\mathbb{I}, \mathbb{R}^{n,n})$ and

$$\frac{d}{dt}(Q^T(t)E(t)) = Q^T(t)[E(t)T(t) - J(t)Q(t)] + [E(t)T(t) - J(t)Q(t)]^T Q(t);$$

ii) the Hamiltonian function $\mathcal{H}(x) := \frac{1}{2}x^T Q^T E x : C^1(\mathbb{I}, \mathbb{R}^n) \rightarrow C^1(\mathbb{I}, \mathbb{R})$ satisfies $\mathcal{H}(x(t)) \geq h_0 \in \mathbb{R}$ uniformly for all $t \in \mathbb{I}$ and all solutions x of (6);

iii) for all $t \in \mathbb{I}$, $W = W^T \geq 0$, where

$$W := \begin{bmatrix} Q^T R Q & Q^T P \\ P^T Q & S \end{bmatrix} \in C^0(\mathbb{I}, \mathbb{R}^{n+m, n+m}). \quad (7)$$

For a general nonlinear pHDAE of the form (1), and a Hamiltonian function $\mathcal{H}(x)$, one requires that Definition 1 holds locally, i. e. for a given input $u(t)$ and associated trajectory $x(t)$, the Hessian $\mathcal{H}_{xx}(x)$ can be expressed locally as $E^T Q$, where $E = F_{\dot{x}}(t)$, $F_x(t) = (J - R)Q - ET$, $F_u(t) = B - P$, $G_x(t) = (B + P)^T Q$, $G_u(t) = S + N$, with $E, J, Q, R, T \in C^0(\mathbb{I}, \mathbb{R}^{n,n})$, $B, P \in C^0(\mathbb{I}, \mathbb{R}^{n,m})$, $S = S^T$, $N = -N^T \in C^0(\mathbb{I}, \mathbb{R}^{m,m})$. It has been shown in [2] that pHDAEs are invariant under time-varying equivalence transformations, they again satisfy the dissipation inequality (5), and they allow for structure preserving regularization and reformulation as it was suggested for general DAEs in [5, 17]. We will not discuss these general results here, but address them in the specific context of power network models where the equations simplify significantly.

2 A model hierarchy for power networks

In this section we briefly discuss a model hierarchy of several currently used power network models, which we then turn into a pHDAE formulation in the following section.

Consider a power network of n generators and loads, both represented by oscillators, connected through transmission lines. If $A = [a_{jk}] \in \mathbb{R}^{n \times n}$ is the adjacency matrix, then the network can be described by a system of the form

$$\begin{aligned} m_j \dot{\theta}_j \ddot{\theta}_j &= -d_j \dot{\theta}_j^2 - v_j I_j + P_j, & \text{for } 1 \leq j \leq k, \\ L_{jk} \dot{i}_{jk} &= -R_{jk} i_{jk} + v_j - v_k, & \text{for } 1 \leq j < k \leq n, \quad a_{jk} \neq 0, \\ 0 &= -I_j + \sum_{k \neq j} a_{jk} i_{jk}, & \text{for } 1 \leq j \leq n. \end{aligned} \quad (8)$$

where θ_j is the *phase angle* and $v_j = V_j \cos \theta_j$ the *voltage* of the j -th oscillator, with $V_j > 0$ being the *voltage magnitude*; I_j is the *current* passing through the j -th oscillator entering the circuit; i_{jk} is the *current through the transmission line* connecting oscillators j and k ; $P_j \in \mathbb{R}$ is the *exchange of power* of the j -th oscillator with the environment ($P_j > 0$ for generators, $P_j < 0$ for loads); $m_j > 0$ and $d_j > 0$ are the *inertia* and the *damping constant* of the j -th oscillator, respectively; $L_{jk} > 0$ and $R_{jk} > 0$ are the *inductance* and *resistance* of the transmission line connecting oscillators j and k , respectively. Moreover, we assume that m_j , d_j , L_{jk} and R_{jk} are constant in time. This model is called the *instantaneous power model*, since the first equation of (8) represents the power balance of each node at every instant of time.

In many real power network applications, one expects all angular velocities $\dot{\theta}_j$ to be close to a constant reference frequency Ω . Thus, it is often assumed that in given a time interval $\dot{\theta}_j = \Omega$ and that V_j, P_j are constant for all j . If this is the case, then the current i behaves in a very regular way. In this case the second equation in (8) can be approximated well by an algebraic equation, and the electrical power $v_i I_j$ in the first equation of (8) can be replaced by the *real power*, i. e., the average electrical power going through the oscillator during a period of time $1/\Omega$. This leads to the so-called *real power model*

$$m_j \dot{\theta}_j \ddot{\theta}_j = -d_j \dot{\theta}_j^2 - \sum_{k=1}^n r_{jk} \cos(\theta_k - \theta_j) + \sum_{k=1}^n g_{jk} \sin(\theta_k - \theta_j) + P_j,$$

for $j = 1, \dots, n$, where $R = R^T = [r_{jk}] \geq 0$, $G = G^T = [g_{jk}] \leq 0$, depend on the resistances, the inductances, the voltage magnitudes, and the reference frequency of the system. Note that in this model the current i is included only implicitly.

Since often the entries r_{jk} of the resistance matrix are negligible compared to the other coefficients, one can also carry out a further simplification $r_{jk} \equiv 0$. Furthermore, for small time intervals one may substitute some terms $\dot{\theta}_j$ with Ω . This leads (after an appropriate rescaling of the equation by ω^{-1}) to the system

$$m_j \ddot{\theta}_j = -d_j \dot{\theta}_j + \sum_{k=1}^n \tilde{g}_{jk} \sin(\theta_k - \theta_j) + \tilde{P}_j, \quad (9)$$

for $j = 1, \dots, n$, which we call the *generalized Kuramoto model*. It is a generalization of the standard *Kuramoto model* which consists of a system of n fully-coupled oscillators satisfying the equations

$$m_j \ddot{\theta}_j + d_j \dot{\theta}_j = \Omega_j + K \sum_{k=1}^n \sin(\theta_k - \theta_j), \quad (10)$$

for $j = 1, \dots, n$, where θ_j denotes the phase angles, $m_j > 0$ the masses, $d_j > 0$ the dissipation constants, K is the coupling constant, and Ω_j the natural frequencies.

We summarize all the mentioned models in a *model hierarchy*, see Figure 1, where lower level models result from simplifications of the higher levels.

Using such a model hierarchy allows to adapt the model depending on the task, the accuracy requirements, or the allowed computation time. For example, to check stability properties of a synchronous state, the Kuramoto model may be used to achieve high computational efficiency, while the instantaneous power model may be required when accurate quantitative solutions are necessary. Note that the model hierarchy is by no means complete and it should be extended, when further components (like e. g. transformer stations) need to be included, or when the parameters of the system (like e. g. the load) need to be modeled in a stochastic way.

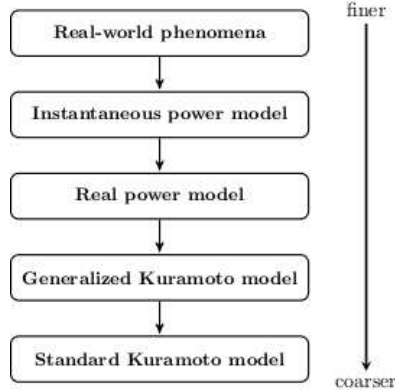


Figure 1: Model hierarchy for power networks

2.1 The order parameter

The standard Kuramoto model is frequently used to study qualitatively the synchronization of power networks [10, 23, 24]. For this one introduces the complex *order parameter*

$$re^{i\phi} = \frac{1}{n} \sum_{j=1}^n e^{i\theta_j} \in [0, 1].$$

The value of r is 1 when the system is in a fully synchronized state and it is 0 when it is completely de-synchronized. Note that

$$r^2 = re^{i\phi} \overline{re^{i\phi}} = \frac{1}{n^2} \sum_{j,k} e^{i(\theta_k - \theta_j)} = \frac{1}{n^2} \sum_{j,k} \cos(\theta_k - \theta_j),$$

so introducing new variables $\omega_j := \dot{\theta}_j$, $\rho_j := \cos \theta_j$, $\sigma_j := \sin \theta_j$, $j = 1, \dots, n$, we obtain

$$\sin(\theta_k - \theta_j) = \sigma_k \rho_j - \sigma_j \rho_k, \quad \cos(\theta_k - \theta_j) = \rho_j \rho_k + \sigma_k \sigma_j,$$

and system (10) takes the form

$$\begin{aligned} \dot{\theta}_j &= \omega_j, \\ m_j \dot{\omega}_j &= \Omega_j - d_j \omega_j + K \rho_j \sum_{k=1}^n \sigma_k - K \sigma_j \sum_{k=1}^n \rho_k. \end{aligned} \quad (11)$$

In this paper we focus on the bottom two levels of the model hierarchy and show that the generalized Kuramoto model has several advantages compared to the standard Kuramoto model. However, to improve the robustness of the representations further, in the next section we will generate an energy based formulation of these two models as port-Hamiltonian differential-algebraic systems (pHDAE).

3 PHDAE formulation of the Kuramoto models

In this section we will consider the standard (10) and the generalized Kuramoto model (9) and reformulate them as pHDAEs. Introducing the vectors and matrices $\theta = [\theta_j]$, $\omega = [\omega_j]$, $\rho = [\rho_j]$, $\sigma = [\sigma_j]$, $\Omega = [\Omega_j]$, $M = \text{diag}(m_j)$, $D = \text{diag}(d_j)$, $D_\rho = \text{diag}(\rho_j)$, $D_\sigma = \text{diag}(\sigma_j)$ and $G = Kee^T$, where $e \in \mathbb{R}^n$ is the vector of all ones, we can write (11) as

$$\begin{aligned} \dot{\theta} &= \omega, \\ M\dot{\omega} &= \Omega - D\omega - D_\sigma G\rho + D_\rho G\sigma. \end{aligned} \quad (12)$$

Introducing the derivatives of ρ and σ , we get $\dot{\rho} = -D_\sigma\omega$, and $\dot{\sigma} = D_\rho\omega$. Since computing ρ and σ is equivalent to determining θ , we can discard the first equation in (12) and obtain a pHDAE formulation $E\dot{x} = (J - R)Qx + Bu$ of the standard Kuramoto model as

$$\begin{aligned} M\dot{\omega} &= \Omega - D\omega - D_\sigma G\rho + D_\rho G\sigma, \\ \dot{\rho} &= -D_\sigma\omega, \\ \dot{\sigma} &= D_\rho\omega, \end{aligned} \tag{13}$$

where $x = [\omega^T, \rho^T, \sigma^T]^T \in \mathbb{R}^{3n}$, $u = \Omega \in \mathbb{R}^n$, $E = \text{diag}(M, I, I) \in \mathbb{R}^{3n \times 3n}$, $0 \leq R = R^T = \text{diag}(D, 0, 0) \in \mathbb{R}^{3n \times 3n}$, $Q = \text{diag}(I, -G, -G) \in \mathbb{R}^{3n \times 3n}$, and

$$J = -J^T = \begin{bmatrix} 0 & D_\sigma & -D_\rho \\ -D_\sigma & 0 & 0 \\ D_\rho & 0 & 0 \end{bmatrix}, \quad B = \begin{bmatrix} I \\ 0 \\ 0 \end{bmatrix}.$$

In contrast to the general formulation of pHDAEs in (6), we have that E and Q are constant in time, and $T = 0$. The *Hamiltonian function* is

$$\mathcal{H}(x) = \frac{1}{2}x^T Q^T E x = \frac{1}{2}\omega^T M\omega - \frac{1}{2}\rho^T G\rho - \frac{1}{2}\sigma^T G\sigma, \tag{14}$$

and, in particular, we have

$$\frac{1}{2}\rho^T G\rho + \frac{1}{2}\sigma^T G\sigma = \frac{1}{2}K \sum_{j,k} (\rho_j \rho_k + \sigma_j \sigma_k) = \frac{1}{2}K \sum_{j,k} \cos(\theta_k - \theta_j) = \frac{1}{2}K n^2 r^2,$$

so that $\mathcal{H}(x) = \frac{1}{2}\omega^T M\omega - \frac{1}{2}K n^2 r^2$.

Since we have omitted the dependence of ρ and σ on θ , the components ρ and σ of the solution x implicitly need to satisfy the property

$$\rho_j^2(t) + \sigma_j^2(t) = 1, \quad \text{for } j = 1, \dots, n \tag{15}$$

for all $t \in \mathbb{I}$, since $\rho_j = \cos(\theta_j)$ and $\sigma_j = \sin(\theta_j)$ for some functions $\theta_1, \dots, \theta_n$.

Unfortunately, when applying numerical integrators to (13), implicit relations like (15) are typically not preserved, due to discretization and roundoff errors, see [18] for a detailed discussion and stabilization techniques to avoid this effect. One way out of this difficulty is to add the conditions (15) explicitly to the system, as n new algebraic equations, making the system overdetermined. To obtain again a pHDAE, we introduce a vector of Lagrange multipliers $\mu = [\mu_j] \in \mathbb{R}^n$. System (13), is then equivalent to the system

$$\begin{aligned} M\dot{\omega} &= \Omega - D\omega - D_\sigma G\rho + D_\rho G\sigma, \\ \dot{\rho} &= -D_\sigma\omega, \\ \dot{\sigma} &= D_\rho\omega, \\ 0 &= D_\rho\rho + D_\sigma\sigma - \mu, \end{aligned} \tag{16}$$

together with initial conditions $x(t_0) = x_0$ satisfying (15), and $\mu(t_0) = e$.

Indeed, by differentiating the fourth equation of (16) with respect to t , and substituting the second and third equation, we get

$$\dot{\mu} = D_\rho\dot{\rho} + D_\sigma\dot{\sigma} = -D_\rho D_\sigma\omega + D_\sigma D_\rho\omega = 0,$$

so $\tilde{x} = [\omega^T, \rho^T, \sigma^T, \mu^T]^T$ is a solution of (16) if and only if $x = [\omega^T, \rho^T, \sigma^T]^T$ is a solution of (13) and μ is constant. System (16) can again be written as pHDAE $\tilde{E}\dot{\tilde{x}} = (\tilde{J} - \tilde{R})\tilde{Q}\tilde{x} + \tilde{B}u$, with

$$\tilde{E} = \begin{bmatrix} E & 0 \\ 0 & 0 \end{bmatrix}, \quad \tilde{J} = \begin{bmatrix} J & 0 \\ 0 & 0 \end{bmatrix}, \quad \tilde{x} = \begin{bmatrix} x \\ \mu \end{bmatrix}, \quad \tilde{Q} = \left[\begin{array}{ccc|c} & & & 0 \\ & Q & & 0 \\ & & & 0 \\ \hline 0 & D_\rho & D_\sigma & -I \end{array} \right], \quad \tilde{R} = \begin{bmatrix} R & 0 \\ 0 & I \end{bmatrix}, \quad \tilde{B} = \begin{bmatrix} B \\ 0 \end{bmatrix}.$$

Note that again $\tilde{J} = -\tilde{J}^T$, and $\tilde{Q}^T \tilde{E} = \tilde{E}^T \tilde{Q}$ do not depend on time. Furthermore,

$$\tilde{Q}^T \tilde{R} \tilde{Q} = \left[\begin{array}{c|c} D & 0 \\ \hline 0 & \begin{bmatrix} D_\rho & D_\rho^T \\ D_\sigma & D_\sigma^T \\ -I & -I \end{bmatrix} \end{array} \right] \geq 0,$$

so the Hamiltonian has not changed.

In an analogous way we can formulate the generalized Kuramoto as a pHDAE. We take a slightly more general approach than in Section 2 and start from a system of n oscillators satisfying the equations

$$m_j \ddot{\theta}_j + d_j \dot{\theta}_j = \Omega_j + \sum_{k=1}^n g_{jk} \sin(\theta_k - \theta_j), \quad (17)$$

for $j = 1, \dots, n$, where g_{jk} are the entries of $G = G^T \in \mathbb{R}^{n \times n}$, satisfying $g_{jk} = g_{kj} \geq 0$ for $j \neq k$. These entries represent the strength of the link between the oscillators j and k , and are 0 when no link is present. The diagonal entries of G can be chosen freely. We will also denote by G_0 the matrix without its diagonal entries, i. e. $G_0 := G - \text{diag}(G)$. Note that if we choose $G = Kee^T$, then we are in the same situation as in the Section 2.

The pHDAE formulation of the generalized Kuramoto system (17) is achieved analogous to that for the standard Kuramoto model, with the Hamiltonian given by (14), where the choice of $\text{diag}(G)$ modifies the Hamiltonian by an additive constant, since

$$-\frac{1}{2} \rho^T G \rho - \frac{1}{2} \sigma^T G \sigma = -\frac{1}{2} \rho^T G_0 \rho - \frac{1}{2} \sigma^T G_0 \sigma - \frac{1}{2} \sum_{j=1}^n g_{jj} (\rho_j^2 + \sigma_j^2),$$

and thus

$$-\frac{1}{2} \rho^T G \rho - \frac{1}{2} \sigma^T G \sigma = -\frac{1}{2} \sum_{j,k} g_{jk} (\rho_j \rho_k + \sigma_j \sigma_k) = -\frac{1}{2} \sum_{j,k} g_{jk} \cos(\theta_k - \theta_j)$$

takes the role of $-\frac{1}{2} n^2 r^2$ in the Hamiltonian.

3.1 The generalized order parameter

The modification of the Hamiltonian by an additive constant in the pHDAE formulation of the generalized Kuramoto model suggests to also define a *generalized order parameter* of the form

$$\xi := \frac{1}{c} \sum_{j,k} g_{jk} \cos(\theta_k - \theta_j) + b,$$

with real constants $b, c > 0$, possibly depending on G , which take the role of r^2 in the standard Kuramoto model. Using the generalized order parameter, the Hamiltonian can be written as

$$\mathcal{H} = \frac{1}{2} \omega^T M \omega + \frac{1}{2} c (b - \xi),$$

where b, c need to be chosen to retain consistency with the standard Kuramoto model.

Note that we still have freedom in choosing the diagonal entries of the matrix G , that have no influence in the differential equation, and that change ξ and the Hamiltonian \mathcal{H} in the same way that b does.

Lemma 2. *Consider the pHDAE formulation of (17) with generalized order parameter ξ . Then the maximal value of $\xi(\theta)$ is given by $c^{-1} \sum_{j,k} g_{jk} + b$, and the maximum is achieved if and only if each connected component of the network, whose topology is defined using G as (weighted) adjacency matrix, is fully synchronized.*

Proof. Since $c > 0$, $g_{jk} \geq 0$ for $j \neq k$, and $\cos(\theta_k - \theta_j) \leq 1$, it is clear that for all $\theta \in \mathbb{R}^n$ we have

$$\xi(\theta) \leq c^{-1} \sum_{j,k} g_{jk} + b.$$

Equality holds if and only if $\theta_j \equiv \theta_k \pmod{2\pi}$ for all j, k such that $g_{jk} \neq 0$. This condition is equivalent to the following statement. If there is a path through the network defined by G that connects j and k , then $\theta_j \equiv \theta_k \pmod{2\pi}$. In turn, this property is equivalent to the full synchronicity of all connected components. \square

If we want to preserve the property that $\max_{\theta} \xi(\theta) = 1$, then we must require that $c(1 - b) = \sum_{j,k} g_{jk}$, or equivalently $c(1 - b) - \sum_j g_{jj} = e^T G_0 e$. We can also force the Hamiltonian \mathcal{H} to be non-negative, with minimum value 0, by choosing $b = 1$, i. e. $\sum_j g_{jj} = -e^T G_0 e$.

Lemma 3. *Suppose that $b = 1$ and $g_{jj} = -\sum_{k \neq j} g_{jk}$ for $j = 1, \dots, n$. Then $\max_{\theta} \xi(\theta) = 1$, $\min_x \mathcal{H}(x) = 0$, and $G \leq 0$ is singular.*

Proof. The particular choice of b and g_{jj} gives the first two assertions. We also have $Ge = 0$, so G is singular and finally, $G \leq 0$ is an immediate consequence of the Gersgorin theorem [12]. \square

To illustrate the previous analysis we present some examples.

Example 4. Consider the standard Kuramoto model with $G_0 = Kee^T - I$. Choose $b = 1$ and $g_{jj} = K(1 - n)$ for $j = 1, \dots, n$, i. e. $G = G_0 - (n - 1)KI = K(ee^T - nI)$. To obtain $c > 0$ such that $\xi = r^2$, we note that

$$\xi = \frac{1}{c} \left(\sum_{j=1}^n (g_{jj} - K) + K \sum_{j,k} \cos(\theta_k - \theta_j) \right) + 1 = \frac{1}{c} (-Kn^2 + Kn^2 r^2) + 1 = \frac{Kn^2}{c} (r^2 - 1) + 1,$$

so $c = Kn^2$ gives $\xi = r^2$ and $\mathcal{H} = \frac{1}{2}\omega^T M\omega + \frac{1}{2}Kn^2(1 - r^2)$.

In the following, we always assume that $b = 1$ and $g_{jj} = -\sum_{k \neq j} g_{jk}$ for $j = 1, \dots, n$. It would be interesting to choose $c(G_0)$ in such a way that $\min_{\theta} \xi(\theta) = 0$ for each choice of G_0 , but it is not clear how this can be achieved, since

$$\min \left(\sum_{j,k} g_{jk} \cos(\theta_k - \theta_j) \right)$$

depends strongly on the topology and on the weights of the network.

Example 5. Consider a network with 3 oscillators

$$G_0 = \begin{bmatrix} 0 & 1 & 1 \\ 1 & 0 & 0 \\ 1 & 0 & 0 \end{bmatrix}, \quad G = \begin{bmatrix} -2 & 1 & 1 \\ 1 & -1 & 0 \\ 1 & 0 & -1 \end{bmatrix}.$$

While in the standard Kuramoto model the minimum of ξ was attained for $e^{i\theta_j}$, evenly distributed on the unit circle for $j = 1, 2, 3$, now it is attained for $e^{i\theta_2} = e^{i\theta_3} = -e^{i\theta_1}$ instead. Indeed, this condition gives that for all j, k such that $j \neq k$ and $g_{jk} \neq 0$, we have $\cos(\theta_k - \theta_j) = -1$, a configuration that was not achievable in the fully coupled case. In this special case we have

$$\sum_{j,k} g_{jk} \cos(\theta_k - \theta_j) = -\sum_{j,k} |g_{jk}| = -8,$$

while choosing the $e^{i\theta_j}$ evenly distributed would give only

$$\sum_{j,k} g_{jk} \cos(\theta_k - \theta_j) = -6.$$

A similar effect would also happen if we choose

$$G_0 = \begin{bmatrix} 0 & 1 & 1 \\ 1 & 0 & \varepsilon \\ 1 & \varepsilon & 0 \end{bmatrix},$$

with $\varepsilon > 0$ very small.

Since, depending on G , we could have

$$\sum_{j,k} g_{jk} \cos(\theta_k - \theta_j) = - \sum_{j,k} |g_{jk}| = -2e^T G_0 e,$$

one may be tempted to always choose $c = -2e^T G_0 e$, but this would not be consistent with the standard Kuramoto model, since then we would have $\min_{\theta} \xi(\theta) > 0$. Since in the standard Kuramoto model we have

$$e^T G_0 e = K(n^2 - n) = Kn^2 \frac{n-1}{n} = c \frac{n-1}{n},$$

we may define in general

$$c(G_0) = \frac{n}{n-1} e^T G_0 e = \left(1 + \frac{1}{n-1}\right) e^T G_0 e,$$

to guarantee consistency with the standard Kuramoto model. With this choice, we obtain

$$\xi(\theta) = 1 - \frac{n-1}{n} \frac{\sum_{j,k} g_{jk} \cos(\theta_k - \theta_j)}{e^T G_0 e} \geq 1 - 2 \frac{n-1}{n} = -1 + \frac{2}{n},$$

so we can guarantee that $\xi \in [-1 + \frac{2}{n}, 1]$, in particular $|\xi| \leq 1$.

3.2 Relative phase angle formulation

To analyze the dynamics of the system, it is sufficient to consider the relative phase angles $\theta_j - \theta_k$ for $j, k = 1, \dots, n$, instead of the absolute phase angles θ_j for $j = 1, \dots, n$. This has the advantage that it removes some redundancy from the system. For example, if two states (θ, ω) and $(\theta + \gamma e, \omega)$, with $\theta, \omega \in \mathbb{R}^n$ and $\gamma \in \mathbb{R}$, that behaved in the same way in the old system, they are coincident in the new system. To simplify the presentation, for the remainder of this subsection, we suppose to have $n+1$ oscillators $\theta_0, \dots, \theta_n$ instead of n . Then considering all phase angles relative to θ_0 , setting

$$\hat{\theta}_j := \theta_j - \theta_0, \quad \hat{\rho}_j := \cos(\hat{\theta}_j), \quad \hat{\sigma}_j := \sin(\hat{\theta}_j), \quad j = 1, \dots, n,$$

and $\hat{\theta}_0 = 0, \hat{\rho}_0 = 1$ and $\hat{\sigma}_0 = 0$, we obtain that

$$\begin{aligned} \cos(\theta_k - \theta_j) &= \cos(\hat{\theta}_k - \hat{\theta}_j) = \hat{\rho}_j \hat{\rho}_k + \hat{\sigma}_j \hat{\sigma}_k, \\ \sin(\theta_k - \theta_j) &= \sin(\hat{\theta}_k - \hat{\theta}_j) = \hat{\rho}_j \hat{\sigma}_k - \hat{\sigma}_j \hat{\rho}_k \end{aligned} \tag{18}$$

are satisfied for $j, k = 0, \dots, n$. This leads to the system

$$\begin{aligned} m_0 \dot{\omega}_0 &= -d_0 \omega_0 + \sum_{k=1}^n g_{0,k} \hat{\sigma}_k + \Omega_0, \\ m_j \dot{\omega}_j &= -d_j \omega_j + \hat{\rho}_j \sum_{k=1}^n g_{j,k} \hat{\sigma}_k - \hat{\sigma}_j \left(\sum_{k=1}^n g_{j,k} \hat{\rho}_k + g_{k,0} \right) + \Omega_j, \quad j = 1, \dots, n \\ \dot{\hat{\rho}}_j &= -(\omega_j - \omega_0) \hat{\sigma}_j, \quad j = 1, \dots, n \\ \dot{\hat{\sigma}}_j &= (\omega_j - \omega_0) \hat{\rho}_j, \quad j = 1, \dots, n. \end{aligned}$$

Introduce

$$G = \begin{bmatrix} g_{00} & g_0^T \\ g_0 & \hat{G} \end{bmatrix}, \quad g_{00} \in \mathbb{R}, \quad g_0 \in \mathbb{R}^n, \quad \hat{G} \in \mathbb{R}^{n \times n}.$$

and choose the diagonal as in the previous subsection. If the vector of all ones is in the kernel of G , then $g_0 = -\hat{G}e$ and $g_{00} = -e^T g_0 = e^T \hat{G}e$. Let us define $\hat{\omega} = [\omega_j]_{j=1, \dots, n} \in \mathbb{R}^n$, $\hat{M} = \text{diag}(m_j)_{j=1, \dots, n}$, $\hat{D} = \text{diag}(d_j)_{j=1, \dots, n}$, $\hat{\Omega} = [\Omega_j]_{j=1, \dots, n} \in \mathbb{R}^n$, $\hat{\rho} = [\hat{\rho}_j] \in \mathbb{R}^n$, $\hat{\sigma} = [\hat{\sigma}_j] \in \mathbb{R}^n$, $D_{\hat{\rho}} = \text{diag}(\hat{\rho})$ and $D_{\hat{\sigma}} = \text{diag}(\hat{\sigma})$, then the system can then be written equivalently as

$$\begin{aligned} m_0 \dot{\omega}_0 &= -d_0 \omega_0 - e^T \hat{G} \hat{\sigma} + \Omega_0, \\ \hat{M} \dot{\hat{\omega}} &= -\hat{D} \hat{\omega} + D_{\hat{\rho}} \hat{G} \hat{\sigma} + D_{\hat{\sigma}} \hat{G} (e - \hat{\rho}) + \hat{\Omega}, \\ \dot{\hat{\rho}} &= -D_{\hat{\sigma}} \hat{\omega} + \hat{\sigma} \omega_0, \\ \dot{\hat{\sigma}} &= D_{\hat{\rho}} \hat{\omega} - \hat{\rho} \omega_0. \end{aligned}$$

Introducing the new variable $\tilde{\rho}_j = 1 - \hat{\rho}_j$ instead of $\hat{\rho}_j$, for $j = 1, \dots, n$, and correspondingly $\tilde{\rho} \in \mathbb{R}^n$ and $D_{\tilde{\rho}} \in \mathbb{R}^{n \times n}$, we obtain the new system

$$\begin{aligned} m_0 \dot{\omega}_0 &= -d_0 \omega_0 - \hat{\sigma}^T \hat{G} \tilde{\rho} - \hat{\rho}^T \hat{G} \hat{\sigma} + \Omega_0, \\ M \dot{\hat{\omega}} &= -D \hat{\omega} + D_{\tilde{\rho}} \hat{G} \hat{\sigma} + D_{\hat{\sigma}} \hat{G} \tilde{\rho} + \Omega, \\ \dot{\tilde{\rho}} &= D_{\hat{\sigma}} \hat{\omega} - \hat{\sigma} \omega_0, \\ \dot{\hat{\sigma}} &= D_{\tilde{\rho}} \hat{\omega} - \tilde{\rho} \omega_0, \end{aligned}$$

that is again a pHDAE system of the form $\hat{E} \dot{\hat{x}} = (\hat{J} - \hat{R}) \hat{Q} \hat{x} + \hat{B} \hat{u}$, with

$$\begin{aligned} \hat{E} &= \begin{bmatrix} m_0 & 0 & 0 & 0 \\ 0 & M & 0 & 0 \\ 0 & 0 & I & 0 \\ 0 & 0 & 0 & I \end{bmatrix}, \quad \hat{Q} = \begin{bmatrix} 1 & 0 & 0 & 0 \\ 0 & I & 0 & 0 \\ 0 & 0 & -\hat{G} & 0 \\ 0 & 0 & 0 & -\hat{G} \end{bmatrix}, \quad \hat{x} = \begin{bmatrix} \omega_0 \\ \hat{\omega} \\ \tilde{\rho} \\ \hat{\sigma} \end{bmatrix}, \quad \hat{u} = \begin{bmatrix} \Omega_0 \\ \Omega \end{bmatrix}, \\ \hat{J} &= \begin{bmatrix} 0 & 0 & \hat{\sigma}^T & \hat{\rho}^T \\ 0 & 0 & -D_{\hat{\sigma}} & -D_{\tilde{\rho}} \\ -\hat{\sigma} & D_{\hat{\sigma}} & 0 & 0 \\ -\tilde{\rho} & D_{\tilde{\rho}} & 0 & 0 \end{bmatrix}, \quad \hat{R} = \begin{bmatrix} d_0 & 0 & 0 & 0 \\ 0 & D & 0 & 0 \\ 0 & 0 & 0 & 0 \\ 0 & 0 & 0 & 0 \end{bmatrix}, \quad \hat{B} = \begin{bmatrix} 1 & 0 \\ 0 & I \\ 0 & 0 \\ 0 & 0 \end{bmatrix}, \end{aligned}$$

with Hamiltonian

$$\mathcal{H}(\hat{x}) = \frac{1}{2} \hat{x}^T \hat{Q}^T \hat{E} \hat{x} = \frac{1}{2} m_0 \omega_0^2 + \frac{1}{2} \hat{\omega}^T M \hat{\omega} - \frac{1}{2} \tilde{\rho}^T \hat{G} \tilde{\rho} - \frac{1}{2} \hat{\sigma}^T \hat{G} \hat{\sigma}.$$

Note that again $\hat{J} = -\hat{J}^T$, $\hat{R} = \hat{R}^T \geq 0$ and $\hat{Q}^T \hat{E}$ is symmetric and does not depend on time.

We observe that, by applying property (18), we get

$$\begin{aligned} \sum_{j,k=0}^n g_{jk} \cos(\theta_k - \theta_j) &= [e \ \hat{\rho}^T] \begin{bmatrix} g_{00} & g_0^T \\ g_0 & \hat{G} \end{bmatrix} \begin{bmatrix} 1 \\ \hat{\rho} \end{bmatrix} + [0 \ \hat{\sigma}^T] \begin{bmatrix} g_{00} & g_0^T \\ g_0 & \hat{G} \end{bmatrix} \begin{bmatrix} 0 \\ \hat{\sigma} \end{bmatrix} \\ &= g_{00} + 2g_0^T \hat{\rho} + \hat{\rho}^T \hat{G} \hat{\rho} + \hat{\sigma}^T \hat{G} \hat{\sigma} \\ &= e^T \hat{G} e - 2e^T \hat{G} \hat{\rho} + \hat{\rho}^T \hat{G} \hat{\rho} + \hat{\sigma}^T \hat{G} \hat{\sigma} \\ &= (e - \hat{\rho})^T \hat{G} (e - \hat{\rho}) + \hat{\sigma}^T \hat{G} \hat{\sigma} \\ &= \tilde{\rho}^T \hat{G} \tilde{\rho} + \hat{\sigma}^T \hat{G} \hat{\sigma}, \end{aligned}$$

so the Hamiltonian is not changed.

Finally, as in the case of the standard Kuramoto model, we incorporate the algebraic equations

$$\hat{\rho}_j^2 + \hat{\sigma}_j^2 = 1, \quad j = 1, \dots, n$$

or equivalently

$$-(1 + \hat{\rho}_j)\tilde{\rho}_j + \hat{\sigma}_j^2 = 0, \quad j = 1, \dots, n.$$

We again introduce Lagrange multipliers $\mu \in \mathbb{R}^n$ and obtain

$$-(I + D_{\hat{\rho}})\tilde{\rho} + D_{\hat{\sigma}}\sigma + \mu = 0.$$

Proceeding analogous as in the reformulation of the standard Kuramoto model, we obtain a modified pHDAE formulation with

$$\begin{bmatrix} \hat{E} & 0 \\ 0 & 0 \end{bmatrix}, \left[\begin{array}{c|c} \hat{Q} & 0 \\ \hline 0 & 0 \end{array} \right], \begin{bmatrix} \hat{J} & 0 \\ 0 & 0 \end{bmatrix}, \begin{bmatrix} \hat{R} & 0 \\ 0 & I \end{bmatrix}, \begin{bmatrix} \hat{B} \\ 0 \end{bmatrix}, \begin{bmatrix} \hat{x} \\ \mu \end{bmatrix},$$

and again the Hamiltonian has not changed.

4 Numerical results

In this section we present some numerical simulation results that illustrate the advantages of our pHDAE formulation. In particular we will concentrate on the Italian high-voltage (380 kV) power grid (Sardinia excluded), which is composed of $N = 127$ nodes, divided in 34 sources (hydroelectric and thermal power plants) and 93 consumers, connected by 342 links [19]. This network is characterized by a quite low average connectivity $N_c = 2.865$, due to the geographical distributions of the nodes along Italy[‡]. As already discussed in Sec. 2, the equation of motion for each node is assumed to be the same for consumers and generators; these are distinguished by the sign of the quantity P_i associated to each node: a positive (negative) P_i corresponds to generators (consumers). For the sake of simplicity, each node is assumed to have the same inertia value ($m_i = m_j = m$, for $i, j = 1, \dots, N$) and the same dissipation constant ($d_i = d_j = d$ for $i = 1, \dots, N$). Moreover, we suppose that $m = M$, $d = D$ and we do not distinguish between the different notations used for the formulation of the Kuramoto rotators and the pHDAE formulation.

4.1 Perfectly balanced bimodal distribution

It is important to stress that in order to have a stable, fully locked state, as a possible solution of Eq. (10), it is necessary that the sum of the generated power equals the sum of the consumed power. Therefore, by assuming that all the generators are identical as well as all the consumers, the distribution of the Ω_i is made of two δ functions located at $\Omega_i = -C$ and $\Omega_i = +G$. In our simulations we have set $C = 1.0$, $G = 2.7353$. This setup corresponds to a Kuramoto model with inertia with a perfectly balanced bimodal distribution of the frequencies. In order to maintain the constraint on the power flow, the same choice for the distribution of the frequencies is made for the pHDAE formulation.

As a first analysis, in order to validate the proposed model, we integrate the set of equations (16) with different integration schemes and compare the results obtained, in particular the conservation of the Lagrange multiplier μ under the different integration schemes. As a reference we use the integration of original equation for the Kuramoto oscillators with inertia Eq. (10) with a 4th order Runge-Kutta scheme with integration step 0.002. On short time intervals the dynamics shown by the system is the same, irrespectively of the integration scheme, however, if we want an exact conservation of the multiplier μ , a geometric integrator like the implicit midpoint method must be applied, taking care of choosing a sufficient accuracy for the nonlinear solver at every integration step. When the accuracy is not sufficient, the multiplier does not remain equal to 1, but its value drifts, as one can see for the explicit midpoint method. On the other hand with the implicit

[‡]The map of the Italian high-voltage power grid can be seen at the web site of the Global Energy Network Institute, <http://www.geni.org>, and the data here employed have been extracted from the map delivered by the union for the coordination of transport of electricity (UCTE), <https://www.entsoe.eu/resources/grid-map/>

midpoint rule, the value of μ does not drift and it is conserved on average, but the instantaneous deviations from 1 are not negligible. For all the integration schemes, the same time step has been used (0.002); it is obvious that the accuracy of the implicit and explicit midpoint can be increased if the time step is decreased at the expense of a larger computing time. The computing time also increases in the implicit midpoint when requiring higher accuracy in the iterative solver.

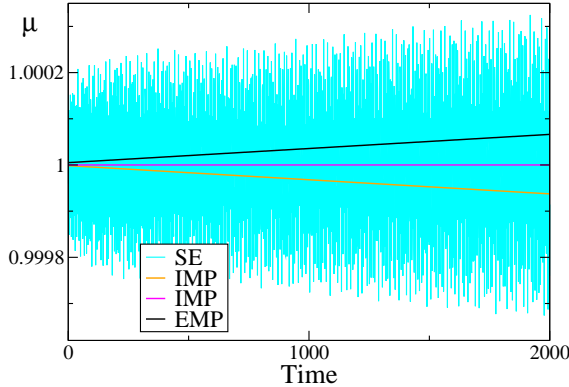


Figure 2: Conservation of the Lagrange multiplier μ for different integration schemes (Symplectic Euler (SE), Implicit Midpoint (IMP), Explicit Midpoint (EMP)). The orange and magenta curves differ for the convergence threshold in the implicit solver (10^{-6} and 10^{-12} , respectively). It is possible to avoid energy drift only applying IMP (with sufficiently small threshold value) and SE. For all the simulations $K = 0.5$, $m = 6$ and $d = 1$, time step 0.002, transient time 100, simulation time 5000.

With the idea in mind to present a new energy-based formulation of the Kuramoto model as port-Hamiltonian system of differential-algebraic equations, it is worth comparing the dynamics emerging in the system of Kuramoto rotators Eqs. (10), with the dynamics of the corresponding port-Hamiltonian system Eqs. (16). If we look at the traces in time of the main variables (e. g. $\theta_i, \dot{\theta}_i$), as well as the traces of the derived variables (e. g. r, ξ), the dynamics is not trivially equal at each time step for the two systems, since we are integrating different sets of equations, but the average values of these variables and the behavior (both at the macroscopic and microscopic levels) are the same. For a coupling constant $K = 2$ the system actually shows a two cluster state, where the rotators are separated into two subsets according to their natural frequency and these two clusters move independently between these frequencies. On the other hand for $K = 20$ the system is completely synchronized and all the rotators move with the same velocity. However, irrespectively of the chosen coupling constant, the models are equivalent.

In order to understand the transition from the non-synchronized state at low coupling constant K to the synchronized state at high K values, we perform sequences of simulations by varying adiabatically the parameter K . A series of simulations is initialized for the decoupled system by considering random initial conditions for $\{\theta_i\}$ and $\{\dot{\theta}_i\}$ (but the same) for both Eqs. (10) and (16). Afterwards the coupling K is increased in small steps until a maximal coupling is reached. For each value of K , apart the very first one, the simulation is initialized by employing the last configuration of the previous simulation in the sequence.

As a first analysis we have calculated the average order parameters \bar{r} , $\bar{\xi}^{1/2}$ by varying the parameter K and we have found that both show a non-monotonic behavior in K (Fig. 3). In particular, for small coupling values $\bar{r} \propto 1/\sqrt{N}$, we observe an abrupt jump for $K = 6.5$ to a finite value; subsequently \bar{r} decreases reaching a minimum at $K = 9$. For larger K the order parameter \bar{r} increases steadily with K tending towards the fully synchronized regime. There are no substantial differences between the Kuramoto order parameter r calculated within the original and the pHDAE formulation, as results from the average values reported in Fig. 3, respectively the dashed magenta curve and the black dots curve. The average order parameter $\bar{\xi}^{1/2}$, on the other hand, does

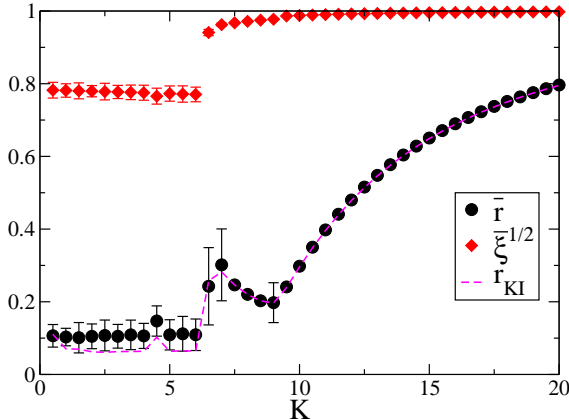


Figure 3: Average order parameters vs the coupling constant K . r_{KI} is the average standard Kuramoto parameter, calculated through a 4th order Runge-Kutta method with the original formulation. \bar{r} and $\bar{\xi}^{1/2}$ are the average standard Kuramoto parameter and generalized over parameter respectively, obtained with the explicit midpoint rule applied to the pHDAE formulation. For all these simulations the inertia term is chosen equal to 6 and the dissipation term to 1. The distribution of the Ω_i is made of two δ functions located at $\Omega_i = C$ and $\Omega_i = +G$. In our simulations we have set $C = 1.0$, $G = 2.7353$. Other parameters as in Fig. 2.

not show such an irregular behavior for small coupling values, but has a constant value until $K = 6.5$, where the transition to synchronization takes place and, from that value on, it rapidly increases towards 1. Since ξ takes into account the topology of the network by introducing the connectivity matrix into the definition and summing over the connected nodes, the investigation of the synchronization level is more straightforward with this new order parameter introduced within the pHDAE formulation: its behavior is more stable for small coupling constants, where it describes better than r the real level of synchronization present into the network, while it is able to identify the transition to synchronization at $K = 6.5$, as the classical Kuramoto order parameter.

The correctness of the critical coupling constant value at which the transition to synchronization takes place can be confirmed indirectly by the calculation of the maximal Lyapunov exponent λ_M , which represents a measure of the stability of the system and is a good indicator for the emergence of problems in the network. In particular, λ_M shows bigger fluctuations before the transitions (Fig. 4), while it is exactly zero when the synchronized state is achieved at $K = 6.5$.

The reason why \bar{r} fails in identifying the correct level of synchronization, can be understood by examining the average phase velocity of the oscillators $\langle \dot{\theta}_i \rangle$ (see Fig. 5). For coupling $K < 6.5$ the system is split in two clusters: one composed by the sources which oscillates with their proper frequency G and the other one containing the consumers, which rotates with average velocity $\langle \dot{\theta}_i \rangle$. Therefore, there is a non-trivial form of partial synchronization already present into the network that it is not taken into account by \bar{r} , whose value of the order of $1/\sqrt{N}$ means that the system behaves asynchronously and the single elements of the network oscillate independently one from the others. For $K = 6.5$ the coupling is sufficient to induce frequency adaptation and to enhance synchronization: the two clusters start merging to a single cluster, although a big part of the oscillators are still not synchronized. For $K = 7$ the oscillators get more entrained, and most of them are locked with almost zero average velocity; however, a large part (53 out of 127) form a secondary cluster of whirling oscillators with a velocity $\langle \dot{\theta} \rangle \simeq -0.122$. This secondary cluster has a geographical origin, since it includes power stations and consumers located in the central part and southern part of Italy, Sicily included, as already seen in [23]. By increasing the coupling to $K = 7.5$ the two clusters merge in a unique cluster with few scattered oscillators and finally, for coupling $K \geq 8$, all the oscillators are locked in a unique cluster, and the increase in the coupling is reflected in a monotonous increase of the average order parameters.

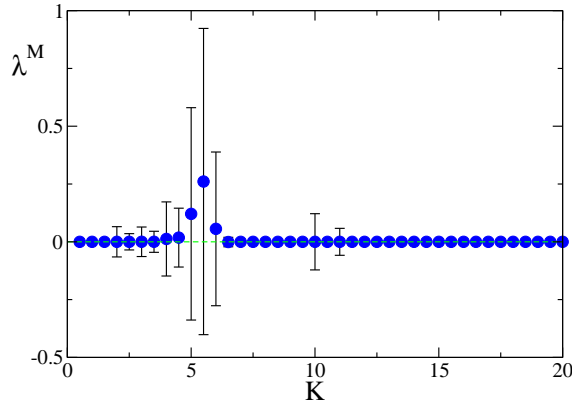


Figure 4: Maximal Lyapunov exponent vs coupling constant K . The dashed green line represents the value $\lambda^M = 0$. For all these simulations the inertia term is chosen equal to 6. The distribution of the Ω_i is made of two δ functions located at $\Omega_i = C$ and $\Omega_i = +G$. In our simulations we have set $C = 1.0$, $G = 2.7353$, $m = 6$ and $d = 1$.

The investigation of the transition to synchronization has been done, up to this point, for a fixed value of the inertia parameter m and of the dissipation constant d , but in order to design proper control schemes able to guide the network towards the synchronization it is necessary to investigate the response of the system for different masses and dissipations. In particular in Fig. 6 the averaged order parameter is displayed as a function of the coupling constant for different masses. For bigger masses the critical coupling value at which the transition to synchronization takes place becomes bigger, thus meaning that bigger coupling strength is necessary in order to achieve the synchronized state for power grid networks in case of bigger masses.

On the other hand bigger dissipation constants help reaching synchronization, as shown in Fig. 7: for fixed coupling values, we can increase the synchronization level by increasing the dissipation d . However, a consistent increase is possible only for coupling constants slightly smaller or bigger than the critical value $K = 6.5$ at which we have observed the transition in Fig. 3, thus illustrating that the coupling strength plays a more important role in the transition with respect to the dissipation parameter. This observation is also justified by the equivalent investigation of the dynamics of the system, obtained by varying the mass m , while keeping constant the coupling strength; in particular the order parameter $\xi^{1/2}$ remains constant for fixed K and does not show any dependence on the mass (results not shown).

When a perturbation takes place into a power grid and a generator is diverging from the synchronized regime at which it is supposed to work, it is important to react to this perturbation as fast as possible in order to avoid having to shut down the generator. The pHDAE formulation of the Kuramoto model with inertia is extremely useful for this kind of problem, thanks to the possibility of fast computation associated to a hierarchical model of the power grid: the differential equations (16) guarantee an on-line fast description of the real system, irrespectively of the fact that it is a simplified model. In particular, the calculation of the maximal Lyapunov exponent can be used to identify instabilities emerging into the network. When it is necessary to operate at the level of the real grid due to emerging disturbances that may affect the stability, the hierarchical model then allows to control and adjust the parameters in more sophisticated models, like the instantaneous power model shown in Sec. 2, and finally into the real grid, by going up along the hierarchy. Starting from a situation where the system is slightly out of synchronization (that is modelled by choosing $K = 6$), we can thus design a control method once the response of the system to the parameters change is known. In particular, we have calculated the time t_s that the system needs to reach the synchronization from this out-of-synchronicity initial condition: if the system is not working perfectly, we can restore the desired status as fast as possible by abruptly

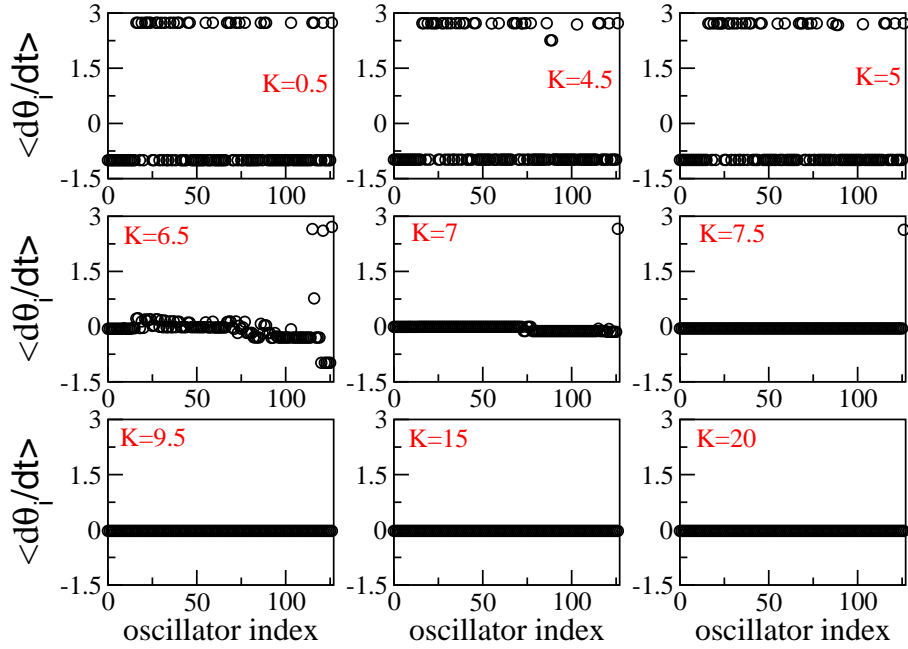


Figure 5: Average phase velocity of each oscillator for different values of the coupling K . The data have been obtained by changing adiabatically the coupling constant, starting from zero coupling $K = 0$ and with $\Delta K = 0.5$. For all the simulations $m = 6$ and $d = 1$. Other parameters as in Figs. 2,3.

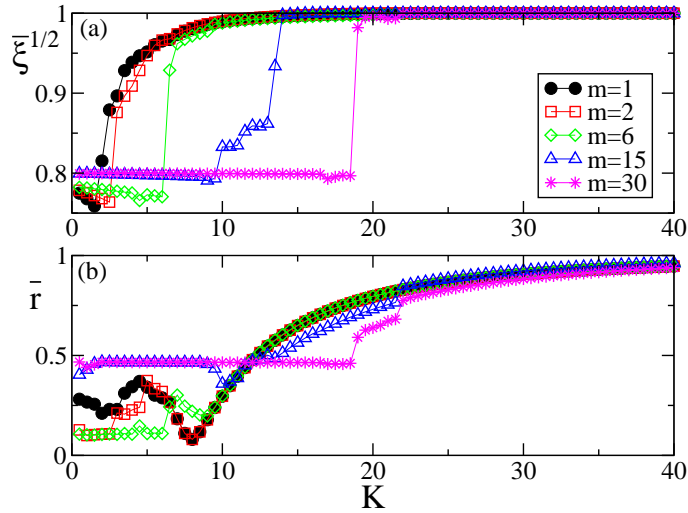


Figure 6: Average order parameters vs the coupling constant K for different masses. In panel (a) (resp. (b)) the average generalized (standard) order parameter is displayed. The data have been obtained by changing adiabatically the coupling constant, starting from zero coupling $K = 0$ and with $\Delta K = 0.5$. Increasing the mass of the system shifts the critical value of the coupling constant at which the system reaches synchronization. For all the simulations $d = 1$.

increasing the coupling constant and the dissipation value or by decreasing the mass (see Fig. 8).

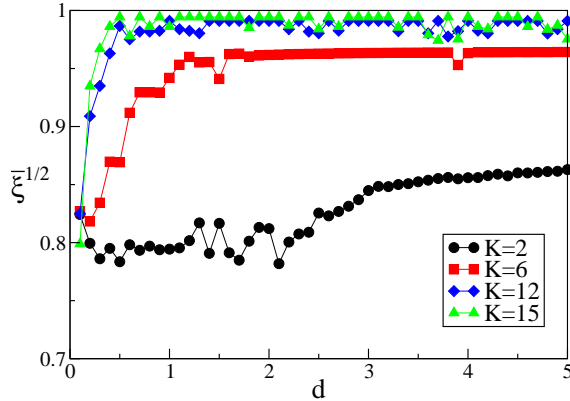


Figure 7: Average order parameter $\bar{\xi}^{1/2}$ vs the dissipation constant d for different coupling constants K . The data have been obtained by changing adiabatically the coupling constant, starting from zero coupling $K = 0$ and with $\Delta K = 0.5$. For all the simulations $m = 6$.

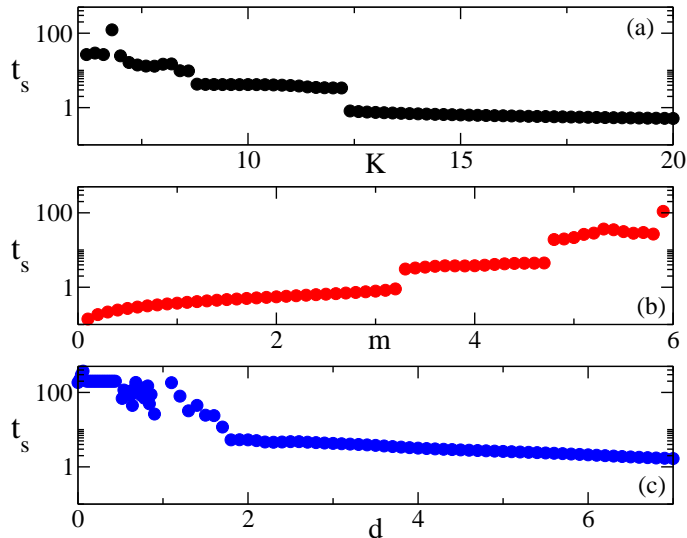


Figure 8: Time t_s necessary to reach a good synchronization state ($\xi^{1/2} > 0.95$), as a function of the parameters. The initial values of the parameters used for these simulations are: $K = 6$, $m = 6$, $d = 1$, while the values K , m , d reported on the x-axes of the panels represent the values to which the initial parameters are tuned in order to calculate the time that the system needs to get synchronized after the non-adiabatic parameter change. In particular the simulations are not obtained by slowly varying the parameters; on the other hand they are obtained re-starting the system always with the same initial conditions, applying abruptly a different change in a single parameter and then calculating the time that the system needs to reach the synchronization.

4.2 Bimodal distribution

In the previous subsection the results have been obtained by choosing frequencies from a bimodal distribution composed of two δ peaks centered at $+G$ and $-C$. Since in the real power grid we do not expect that the natural frequencies of the generators/nodes are characterized by the same exact values, due to the presence of disorder and noise, we discuss now the analysis done with two almost non overlapping Gaussians $g(\Omega) = \frac{1}{2\sqrt{2\pi}} \left[e^{-\frac{(\Omega-\Omega_0)^2}{2}} - e^{-\frac{-(\Omega+\Omega_0)^2}{2}} \right]$ centered at $\Omega_0 = \pm 2$.

The analysis that we have done is equivalent to what is presented in Figs. 3, 4, 5: the investigation of the transition to synchronization and the characterization of the different dynamical behavior emerging for different coupling constants.

The calculation of the average order parameters \bar{r} , $\bar{\xi}^{1/2}$ as a function of the coupling constant reveals that, in this setup, it is more difficult to achieve synchronization, due to the inhomogeneity of the natural frequencies (see Fig. 9). The classical order parameter \bar{r} is always irregular and unstable, irrespectively whether we use the original Kuramoto model or the pHDAE formulation, while $\bar{\xi}^{1/2}$ is more stable and informative. If we concentrate on the behavior of $\bar{\xi}^{1/2}$, we observe a different transition to synchronization with respect to the one in Fig. 3; there is not an evident jump from partial synchronization to almost full synchronization but instead a continuous increase of the synchronicity level into the network. However, in order to obtain the same level of synchronization achieved in Fig. (3), a bigger coupling constant is needed with this new setup.

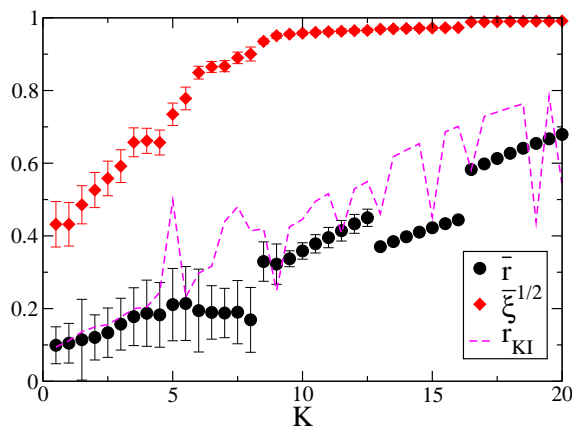


Figure 9: Average order parameters vs the coupling constant K . The parameters values used for these simulations are: $m_j = 6$, $d_j = 1$ for all $j = 1, \dots, N$. The frequencies are chosen according to a bimodal distribution, made of two almost non overlapping Gaussians centered at $\Omega_0 = \pm 2$.

The investigation of the transition in terms of the maximal Lyapunov exponent gives more insight on the transition point from chaotic behavior to synchronization. The critical value of the coupling constant at which the system synchronizes is $K_c = 8.75 \pm 0.25$: for $K > K_c$ the system is stable as testified by the value $\lambda^M = 0$, while for $K < K_c$ the system is chaotic for a wide range of the coupling constant (much wider than in Fig. 4).

Finally the average phase velocity of the oscillators $\langle \dot{\theta}_i \rangle$ is reported in Fig. 11; for small coupling constants the velocities are different and each oscillator moves independently from the others. For $3.5 \leq K \leq 7.5$ some clusters emerge into the networks: the oscillators tend to merge in bigger and bigger clusters, while a many oscillators still remains asynchronous. The cluster synchronization is enhanced by increasing the coupling, while the oscillators that do not get synchronized are usually the ones with higher velocity that adapt their frequency to that of cluster with more difficulty. For $8.5 \leq K < 13$ most of the oscillators are clustered in two or more clusters, while few oscillators are still moving independently. In particular for $K = 8.5$ we have a 3-cluster state plus a limited set of asynchronous oscillators, thus meaning that there are at least 3 effective degrees of freedom acting into the system and contributing to the dynamics; with 3 degrees of freedom it is possible to observe a chaotic motion [30] as confirmed by the positive λ^M for this coupling value. On the other hand it is no more possible to observe chaos for $K > 8.5$, since the system merge into a 2-cluster state; in particular, the dimension of these clusters is very asymmetric and one cluster is much bigger then the second one, thus justifying the increased of the level of synchronization and the corresponding transition to the synchronized state. For bigger coupling constants a single cluster survives and we expect that it will integrate all the oscillators for coupling constants bigger than $K = 20$.

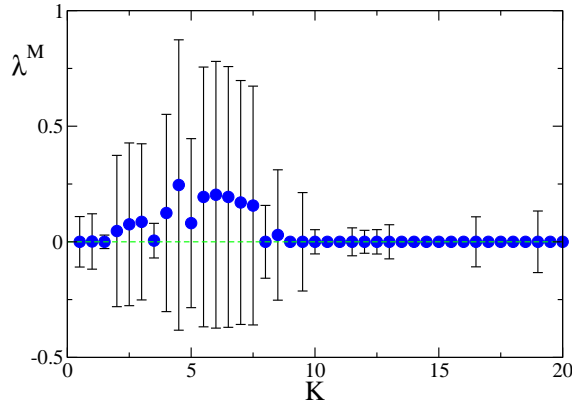


Figure 10: Maximal Lyapunov exponent vs the coupling constant K . The parameters values used for these simulations are: $m_j = 6$, $d_j = 1$ for all $j = 1, \dots, N$. The dashed green line represents the value $\lambda^M = 0$. The frequencies are chosen according to a bimodal distribution, made of two almost non overlapping Gaussians centered at $\Omega_0 = \pm 2$.

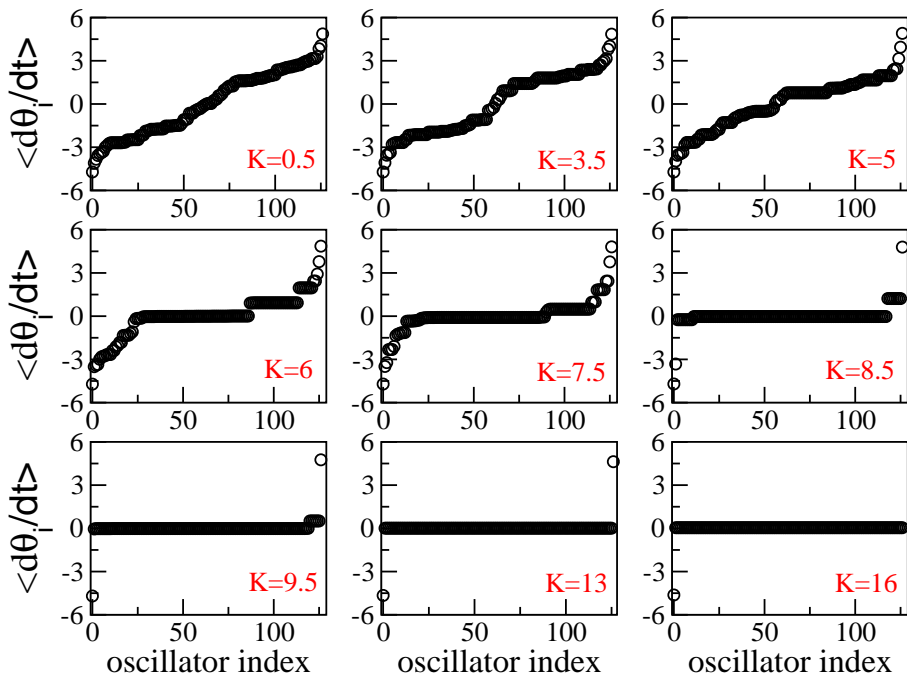


Figure 11: Average phase velocity of each oscillator $\langle \dot{\theta}_i \rangle$ vs the oscillator index for different values of the coupling K . The oscillators are re-named for simplicity so that the averaged phase velocities are plotted in ascending order. The data have been obtained by changing adiabatically the coupling constant, starting from zero coupling $K = 0$ and with $\Delta K = 0.5$. The frequencies are chosen according to a bimodal distribution, made of two almost non overlapping Gaussians centered at $\Omega_0 = \pm 2$.

5 Summary and Outlook

We have presented a new port-Hamiltonian differential-algebraic formulation of the Kuramoto model of coupled oscillators as well as a new definition of the order parameter. The new model

has several advantages, it is easily extended to models of finer granularity as they are used in qualitative stability and synchrony analysis of power systems. The new order parameter is more robust in limiting situations. We have also illustrated the advantage of the port-Hamiltonian formulation in the preservation of conserved quantities. The new approach and its advantages have been illustrated with many numerical examples carried out for a semi-realistic model of the Italian power grid.

Future work will include the analysis of the whole model hierarchy, error control in adaptive time step and model selection, as well as model reduction techniques that allow real time stabilization and synchronization as well as the incorporation of switching in and time-delay in the model.

6 Acknowledgement

V. M. acknowledges the Deutsche Forschungsgemeinschaft via Project A02 within SFB 910 and the *Einstein Foundation Berlin* via the Einstein Center ECMath. R. M. is supported by *Einstein Foundation Berlin* via the Einstein Center ECMath. S. O. and E. S. were supported by DFG via Project A1 in the framework of SFB 910.

References

- [1] C. Beattie and S. Gugercin. Structure-preserving model reduction for nonlinear port-Hamiltonian systems. In *50th IEEE Conference on Decision and Control and European Control Conference (CDC-ECC), 2011*, pages 6564–6569. IEEE, 2011.
- [2] C. Beattie, V. Mehrmann, H. Xu, and H. Zwart. Port-hamiltonian descriptor systems. Preprint xx-2017, Institut für Mathematik, TU Berlin, 2017.
- [3] P. C. Breedveld. *Modeling and Simulation of Dynamic Systems using Bond Graphs*, pages 128–173. EOLSS Publishers Co. Ltd./UNESCO, Oxford, UK, 2008.
- [4] C. I. Byrnes, A. Isidori, and J. C. Willems. Passivity, feedback equivalence, and the global stabilization of minimum phase nonlinear systems. *IEEE Trans. Autom. Control*, 36:1228–1240, 1991.
- [5] S. L. Campbell, P. Kunkel, and V. Mehrmann. Regularization of linear and nonlinear descriptor systems. In L. T. Biegler, S. L. Campbell, and V. Mehrmann, editors, *Control and Optimization with Differential-Algebraic Constraints*, Advances in Control and Design, chapter 2, pages 17–36. 2012.
- [6] J. Cervera, A.J. van der Schaft, and A. Baños. Interconnection of port-Hamiltonian systems and composition of Dirac structures. *Automatica*, 43(2):212–225, 2007.
- [7] F. Couenne, C. Jallut, B. M. Maschke, M. Tayakout, and P. C. Breedveld. Bond graph for dynamic modelling in chemical engineering. *Chemical engineering and processing, Elsevier, Amsterdam*, 47:1994–2003, 2008.
- [8] M. Chertkov F. Doerfler and F. Bullo. Synchronization in complex oscillator networks and smart grids. *Proceedings of the National Academy of Sciences.*, 6(110):2005–10, 2013.
- [9] P. Varaiya F. Salam, J. Marsden. Arnold diffusion in the swing equations of a power system. *IEEE Trans. Circ. Syst.*, 8(31):673–688, 1984.
- [10] G. Filatrella, A. H. Nielsen, and N. F. Pedersen. Analysis of a power grid using a Kuramoto-like model. *The European Physical Journal B*, 61(4):485–491, 2008.

- [11] G. Golo, A. J. van der Schaft, P. C. Breedveld, and B. M. Maschke. Hamiltonian formulation of bond graphs. In A. Rantzer R. Johansson, editor, *Nonlinear and Hybrid Systems in Automotive Control*, pages 351–372. Springer, Heidelberg, 2003.
- [12] G. H. Golub and C. F. Van Loan. *Matrix Computations*. Johns Hopkins Univ. Press, Baltimore, 3rd edition, 1996.
- [13] S. Gugercin, R. V. Polyuga, C. Beattie, and A. J. van der Schaft. Structure-preserving tangential interpolation for model reduction of port-Hamiltonian systems. *Automatica*, 48:1963–1974, 2012.
- [14] D. Hinrichsen and A. J. Pritchard. *Mathematical Systems Theory I. Modelling, State Space Analysis, Stability and Robustness*. Springer-Verlag, New York, NY, 2005.
- [15] B. Jacob and H. Zwart. *Linear port-Hamiltonian systems on infinite-dimensional spaces*. Operator Theory: Advances and Applications, 223. Birkhäuser/Springer Basel AG, Basel CH, 2012.
- [16] P. Kundur, N.J. Balu, and M.G. Lauby. *Power system stability and control*. EPRI power system engineering series. McGraw-Hill, 1994.
- [17] P. Kunkel and V. Mehrmann. *Differential-Algebraic Equations. Analysis and Numerical Solution*. EMS Publishing House, Zürich, Switzerland, 2006.
- [18] P. Kunkel and V. Mehrmann. Stability properties of differential-algebraic equations and spin-stabilized discretizations. *Electron. Trans. Numer. Anal.*, 26:385–420, 2007.
- [19] M. Frasca L. Fortuna and A. Sarra Fiore. A network of oscillators emulating the italian high-voltage power grid. *Int. J. Modern Phys.*, 26:25, 2012.
- [20] R. Lamour, R. März, and C. Tischendorf. *Differential-algebraic equations: a projector based analysis*. Springer Science & Business Media, 2013.
- [21] M. Timme M. Rohden, A. Sorge and D. Witthaut. Self-organized synchronization in decentralized power grids. *Physical Review Letters*, 6(109):064101, 2012.
- [22] T. Nishikawa and A. E. Motter. Comparative analysis of existing models for power-grid synchronization. *New Journal of Physics*, 1(17):015012, 2015.
- [23] S. Olmi, A. Navas, S. Boccaletti, and A. Torcini. Hysteretic transitions in the Kuramoto model with inertia. *Phys. Rev. E*, 90:042905, Oct 2014.
- [24] S. Olmi and A. Torcini. *Dynamics of Fully Coupled Rotators with Unimodal and Bimodal Frequency Distribution*, pages 25–45. Springer International Publishing, Cham, 2016.
- [25] R. Ortega, A. J. van der Schaft, Y. Mareels, and B. M. Maschke. Putting energy back in control. *Control Syst. Mag.*, 21:18–33, 2001.
- [26] R. V. Polyuga and A. J. van der Schaft. Structure preserving model reduction of port-Hamiltonian systems by moment matching at infinity. *Automatica*, 46:665–672, 2010.
- [27] A. J. van der Schaft. Port-Hamiltonian systems: network modeling and control of nonlinear physical systems. In *Advanced Dynamics and Control of Structures and Machines*, CISM Courses and Lectures, Vol. 444. Springer Verlag, New York, N.Y., 2004.
- [28] A. J. van der Schaft. Port-Hamiltonian systems: an introductory survey. In J. L. Verona M. Sanz-Sole and J. Verdura, editors, *Proc. of the International Congress of Mathematicians, vol. III, Invited Lectures*, pages 1339–1365, Madrid, Spain, 2006.

- [29] A. J. van der Schaft. Port-Hamiltonian differential-algebraic systems. In *Surveys in Differential-Algebraic Equations I*, pages 173–226. Springer-Verlag, 2013.
- [30] S. Watanabe and S. H. Strogatz. Constants of motion for superconducting josephson arrays. *Physica D: Nonlinear Phenomena*, 3-4(74):197–253, 1994.
- [31] J. C. Willems. Dissipative dynamical systems – Part I: General theory. *Arch. Ration. Mech. Anal.*, 45:321–351, 1972.
- [32] J. C. Willems. Dissipative dynamical systems – Part II: Linear systems with quadratic supply rates. *Arch. Ration. Mech. Anal.*, 45:352–393, 1972.